Contents

List of Acronyms

NISQ noisy intermediate-scale quantum era

MOT magneto optical trap

ODT optical dipole trap

VQE variational quantum eigensolver

UHV ultra high vacuum

RWA rotating wave approximation

Chapter 1

Introduction

1.1 Quantum Computing

Classical computers have been getting exponentially faster over the last 50 years, as observed by Moore's law [1]. Still, it was suggested as early as 1982 that a classical computer may never be efficient at modeling a quantum mechanical system [2]. This is because of superposition (section 1.1.1) and entanglement (section 1.1.2).

The idea of using a quantum computer is to make use of these very same properties that make a quantum system challenging to simulate, but to use them to one's advantage instead. If this would be possible, we can simulate new molecules and chemical reaction mechanisms, opening up the road to novel medicine [3] and materials [4].

1.1.1 Superposition

Consider a single two level quantum system, quantum bit or 'qubit' $|\psi\rangle$, for example the spin of an electron, which we can define as a basis with basis states $|0\rangle$ (spin up) and $|1\rangle$ (spin down). According to quantum mechanics, this qubit can be in a superposition state [5]:

$$|\psi\rangle = a|0\rangle + b|1\rangle, \tag{1.1}$$

where $a, b \in \mathbb{C}$, where one will measure $|0\rangle$ (spin up in this example) with probability $|a|^2$ and and $|1\rangle$ (spin down) with $|b|^2$. Without loss of generality, we can let the variable θ keep track of the probability of measuring $|0\rangle$ or $|1\rangle$, and defining ϕ as the relatively phase between the two. This is powerful because we can plot the Hilbert space of the qubit on a unit sphere called the Bloch sphere representation [6]

$$|\psi\rangle = \cos\frac{\theta}{2}|0\rangle + e^{i\phi}\sin\frac{\theta}{2}|1\rangle \tag{1.2}$$

This Bloch sphere is shown in fig. 1.1. Classical binary bits are shown as well, which in this analogy occupy only the poles of the sphere, whereas the quantum state can be anywhere on this unit sphere. This is the first hint of the computational potential of a quantum computer. But to build a quantum computer, we are going to need more than one qubit. While we cannot easily graphically represent multi qubit states like for the Bloch sphere, we can still write them down, for which we will introduce the concept entanglement.

1.1.2 Entanglement

We will extend from 1 to 2 electrons. Now, they can be independently spin up $|0\rangle$ and down: $|1\rangle$, for a total of 4 basis states. Quantum physics teaches us this system can be in a superposition of all its basis states [6]:

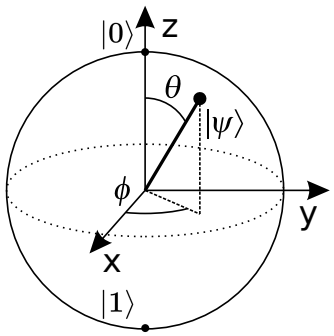

Fig. 1.1: The Bloch sphere representation. A classical bit can only be $|0\rangle$ or $|1\rangle$, whereas a qubit can occupy any point on the sphere with coordinates θ, ϕ. Figure adapted from [7].

$$|\psi_{2q}\rangle = \alpha_{00}|00\rangle + \alpha_{01}|01\rangle + \alpha_{10}|10\rangle + \alpha_{11}|11\rangle. \tag{1.3}$$

Where $|00\rangle$ is shorthand notation for both qubits being in the spin up state, etc. In general, the size of the Hilbert space will grow as 2^N for N qubits [8, 6]. For $N = 300$, this is already larger than the estimated amount of particles in the observable universe at some $\sim 10^{80}$. However, to really access the full Hilbert space, the qubits need to be entangled. These are an inherent quantum feature, having no classical analogue. One of the most instructive examples of an entangled state is

$$|\Phi^+\rangle = \frac{1}{\sqrt{2}}|00\rangle + \frac{1}{\sqrt{2}}|11\rangle \tag{1.4}$$

This is one of the so called Bell states [6] and it is said to be entangled: upon measuring just one of the qubits we immediately know the state of the other qubit as well. This implies the qubits are correlated and cannot be described as a product of independent single qubits. In the operation of a quantum computer, entanglement is a crucial step during the computation stage [8].

1.2 The NISQ Era

Constructing a quantum computer is challenging because apart from full control over each qubit, they should ideally not interact with the environment at all, as this can change their quantum state. This is effect is known as decoherence [9].

Decoherence errors can be corrected but this requires a significant overhead in the available number of qubits and is unachievable in the near term [10, 11]. Therefore, quantum computing is currently in the noisy intermediate-scale quantum era (NISQ) [12]. Noisy refers to the notion that the measured probability amplitudes of the qubits may be slightly different than theoretically expected. The amount of noise can be quantified in a number known as the fidelity, a number between 0 and 1 where 1 means perfect control and zero noise.

During the NISQ era, the algorithms that run on quantum computers should be optimized for finite coherence times and fidelities. One algorithm proposed by [13] is thought to run especially well on non error-corrected hardware, so we will briefly describe its basic principle here [14].

1.2.1 The Variational Quantum Eigensolver

The variational quantum eigensolver (VQE) is an hybrid quantum algorithm: by making use of classical hardware it aims to reduce the amount of quantum gates needed, which is advantageous on NISQ era hardware with finite coherence times [14]. Essentially, VQE tries to find approximately the ground state energy of an atom or molecule according to the variational principle [5], which states that the expectation value of a given Hamiltonian $\mathcal{H}$ will always be an upper bound for the ground state energy E_g:

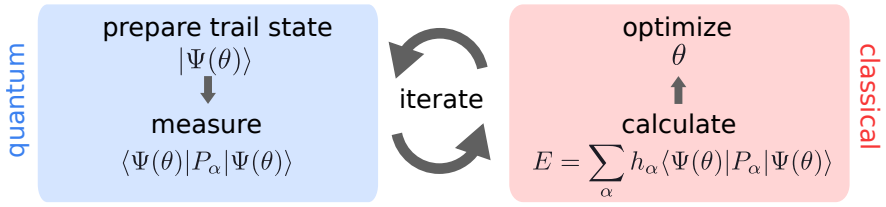

Fig. 1.2: The VQE visualized. Meant to run on a hybrid quantum computer, starting from an ansatz for the wave function it is prepared and the expectation function of its energy measured by a series of measurements on the QPU. Next, a CPU uses a non-linear optimization to find a new ansatz that will decrease the expectation value of $\mathcal{H}$. Iterated until convergence. Figure adapted from [15]

$$\langle\mathcal{H}\rangle = \langle\Psi|\mathcal{H}|\Psi\rangle \geq E_g. \tag{1.5}$$

This is equivalent to finding the eigenvalues of the matrix $\mathcal{H}$. Even for a relatively simple molecules, $\mathcal{H}$ quickly becomes large and the task op diagonalizing it intractable, at least for a classical computer. In VQE, $\mathcal{H}$ is not directly diagonalized but the Hamiltonian is prepared in a quantum co-processor or quantum processing unit (QPU) [8, 13], taking advantage of the large Hilbert state of the quantum hardware.

Given an ansatz θ, a trial state $|\Psi(\theta)\rangle$ is prepared. The Hamiltonian is written in the form of a sum of Pauli strings: P_α with weights h_α [14, 15]

$$\mathcal{H} = \sum_\alpha h_\alpha P_\alpha \tag{1.6}$$

The Pauli string is essentially a tensor product of Pauli spin matrices, the definition is given in appendix A. Because of the decomposition in Pauli strings, estimating the various terms of the Hamiltonian $\langle\Psi|P_\alpha|\Psi\rangle$ boils down to measuring populations of individual qubits, this is explained in appendix A. The total expectation value of the Hamiltonian is obtained by summing over contributions of the Pauli strings. This is done on classical hardware. Subsequently, a non-linear optimizer is run to minimize the energy using a new trial state, and the cycle repeats [15]. The algorithm is visualized in fig. 1.2. The quantum and classical parts of the algorithms feed into each other, therefore VQE is referred to as a hybrid algorithm.

1.3 Hardware Implementation

Now that we know what type of algorithm we aim to run, we will discuss the choice of the quantum hardware implementation. A list of criteria for this was formulated by [9]. Based on this, several quantum computer realizations have been proposed [11]. Examples include: infrared photons [16], trapped ions [17, 18], electron spins [19] and superconducting currents [20, 21].

1.3.1 Neutral Atoms

At TU/e, we aim to build a quantum computer based on qubit states encoded in the electronic states of neutral atoms. The atoms are assembled in arbitrary geometries using laser cooling an trapping techniques. This technique is thought to easily scale to higher number of qubits by increasing the trapping laser power [8].

The atoms are held in place by optical dipole traps [22], each trap is non-deterministically loaded with single atoms [23]. Multiple dipole traps spaced a couple of micro meters from each other are made using holography techniques [24]. Quantum gates and measurements are performed by exciting to Rydberg states and applying Rabi pulses [25, 26]. Qubit states are detected using probe laser pules. A schematic overview of the different steps in neutral atom quantum computing are shown in fig. 1.3.

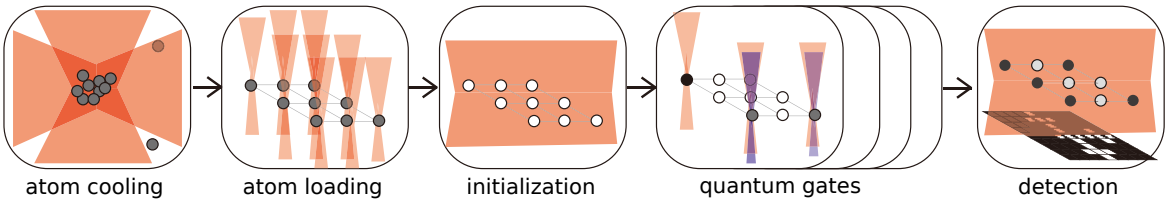

Fig. 1.3: A schematic drawing of the different steps involved in running a QPU based on neutral atoms in optical tweezers, excited to Rydberg states. Starting with a cloud of ultracold atom, the atoms are loaded in an array and the qubits are initialized. Gate operations, as well as readout measurements are performed by applying various laser pulses. Figure from [27].

1.4 This Thesis

In a collaboration with the *Schreck* group at the University of Amsterdam, we aim to realize a NISQ era quantum processing unit. The machine will feature ultracold strontium atoms trapped in arrays of tightly focused laser beams or optical tweezers. This platform has recently shown to achieve high-fidelity quantum gates and measurements [26]. The purpose of this thesis is to give an insight in the first steps carried out at Eindhoven University of Technology towards this goal, which at the time of writing mostly concerns the first two steps in fig. 1.3. In order to do this this work is organized in the following way:

- Background information about laser cooling and trapping techniques, as well as for strontium specifically is presented in chapter 2.
- How we make an optical tweezer inside a vacuum chamber is described in chapter 3.
- Chapter 4 elaborates on how to make arrays in arbitrary geometries using holography techniques.
- Finally, in chapter 5 we describe how to implement the setup in an ultracold atoms experiment.

Chapter 2

Laser Cooling and Trapping

In assembly, computation and readout of single atoms, laser cooling and trapping techniques play a central role. This chapter will give some background on how this technique works, and how we intend to apply it onto strontium (Sr).

2.1 Magneto Optical Trap

The workhorse for producing clouds of ultracold atom is the 3D magneto optical trap (MOT). In essence it, consists of three sets of counter-propagating beams as well as as magnetic field gradient, together providing a dampening as well as a confining force.

2.1.1 Doppler Cooling

Consider an atom with ground state $|g\rangle$ and excited state $|e\rangle$ separated by an energy splitting $\hbar\omega_0$. We drive a laser with omega ω that is near resonant, but *detuned* slightly from the transition by an amount δ:

$$\delta = \omega - \omega_0 \tag{2.1}$$

It will turn out that the detuning is one of the most important parameters in laser cooling. Typically, $\delta < 0$. Because of the Doppler effect, the atom 'sees' a slightly different light frequency depending on its velocity v according to $\delta' = \delta + kv$ and it is possible that the laser becomes resonant: $\delta' = \omega_0$, causing the atom to absorb a photon absorbing momentum $\hbar k$ and promoting an electron to the excited state. When spontaneous emission causes the atom to fall back in a time $\tau = 1/\gamma$ where γ is the linewidth of the transition, the electron is decayed back to the ground state, but the emitted photon is emitted in a random direction. This can be repeated many times per second at a scattering rate Γ_{sc} [28]

$$\Gamma_{sc} = \frac{\gamma s_0/2}{1 + s_0 + [2(\delta + kv)/\gamma]^2}, \tag{2.2}$$

where $s_0 = I/I_{sat}$ is the saturation parameter as a function of the light intensity I for saturation intensity $I_{sat} = \hbar c\gamma\pi/3\lambda^3$ for wavelength λ and linewidth γ. Because the absorption occurs in a fixed direction and the emission is a random event, the atom will experience a net force scattering force $F = \hbar k\Gamma_{sc}$.

2.1.2 Optical Molasses

We can reflect the laser beam using a mirror, such that the force works in both directions of the coordinate which we call z. The total force from both contributions from eq. (2.2) is [29]

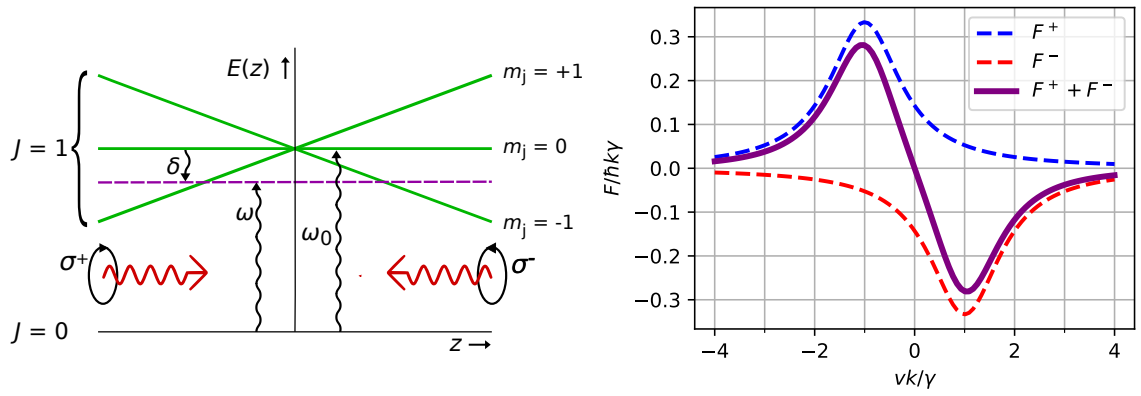

Fig. 2.1: a) Concept of optical molasses in 1D. Atomic frequency is detuned from the atomic transition by $\delta < 0$. Because of the linear magnetic field, at some displacement the $m_j = -1$ atoms become resonant with only σ^+ light because of selection rules, and vice versa. b) Cooling force from a magneto-optical trap. Contributions from the F^+, F^- and the total force are shown for $\delta = -\gamma$ and $I/I_0 = 2$.

$$F = \frac{\hbar k \gamma s_0}{2} \left\{ \left[1 + s_0 + 4\frac{(\delta + kv)^2}{\gamma^2} \right]^{-1} + \left[1 + s_0 + 4\frac{(\delta - kv)^2}{\gamma^2} \right]^{-1} \right\} \tag{2.3}$$

We have plotted the result of eq. (2.3) as a function of velocity in units of $\hbar/k$ to make it dimensionless. Contributions of both beams, as well as their total force are shown in units of $\hbar k\gamma$. Doing a series expansion to first order around $v = 0$. For $\delta < 0$ we find we can linearize the force F as

$$F \approx -\hbar k^2 s_0 \frac{-2\delta/\gamma}{\left[1 + s_0 + (2\delta/\gamma)^2\right]^2} \equiv -\beta v \tag{2.4}$$

Where β is the slope of the scattering force around $v = 0$. Apparently, the resulting force has a dampening character on the velocity, which if applied in all 3 dimensions can effectively cool atoms.

The treatment so far would suggest that this can be used to cool atoms to temperatures of absolute zero. This is not the case, as the random character of the scattering force means the atom fluctuate around the equilibrium velocity according to a Brownian motion. For $\delta = -\gamma/2$, β is at a maximum, yielding the lowest possible temperature achievable using Doppler cooling called the Doppler temperature T_D

$$T_D = \frac{\hbar}{2k_b}\gamma. \tag{2.5}$$

where k_b is Boltzmann's constant. Apparently, this cooling limit is only dependent on the linewidth of the transition γ, apart from physical constants. This result will be used later in section 2.2.

2.1.3 Magnetic Trapping

Apart from cooling the atoms, we want to trap them at a specific location to increase the density of atoms. We can use the Zeeman effect for this, which tells us the atomic energy levels will be split an amount ΔE according to [5]

$$\Delta E = \mu_B g_J m_j B, \tag{2.6}$$

where B is the Bohr magneton, g_J the Landé g-factor, m_j is the magnetic quantum number and B_{ext} the applied magnetic field. The magnetic field is tuned in such a way that is is linear in all 3 dimensions and zero at the center of the MOT by using a set of magnetic field coils in anti-Helmholtz configuration. Because of the Zeeman splitting, the chance of the atoms coming in resonance with the laser vary with the position from the origin according to

$$\delta' = \delta + kv - \frac{\mu' B}{\hbar} \tag{2.7}$$

To ensure that atoms only absorb momentum kicks in the right direction, the laser beams are circularly polarized: σ^+ from the left and σ^- from the right. Because the sign of the Zeeman shift is dependent on the magnetic quantum number m_j, selection rules prescribe. For 3 dimensions the force becomes

$$\frac{F}{\hbar k \gamma s_0} = \frac{1}{2}\left\{ \left[1 + s_0 + 4\frac{(\delta + kv + \mu' B/\hbar)^2}{\gamma^2}\right]^{-1} + \left[1 + s_0 + 4\frac{(\delta - kv - \mu' B/\hbar)^2}{\gamma^2}\right]^{-1} \right\} \tag{2.8}$$

Where $\mu' = (g_e m_e - g_g m_g)\mu_B$ is the effective magnetic moment for the transition [29]. Expanding eq. (2.8) around $(v, z) = (0, 0)$, keeping only first order terms, extending the same concept to the other two dimensions yields finally

$$F_{\text{MOT}}(z, v) \approx -\beta v - \kappa z. \tag{2.9}$$

Where β is the same we found in eq. (2.4) and $\kappa \equiv \mu'\beta/\hbar k \cdot \partial B/\partial z$. Apart from the dampening force, a force with Hookian character arises for linear magnetic field gradient as well. These are the two ingredients for producing high density cold atom clouds.

2.2 Strontium

Historically, people started laser cooling experimentation on group 1 or alkali atoms (Na, Rb, Cs). Because they only have one valence electron, the level structure is relatively straightforward. Also, diode lasers are available for their transition frequencies. This work contains trapping of alkali earth atoms explained in chapter 5.

However, also group 2 atoms, also called alkali-earth (and similar atoms like Yb) are a possible candidate. Because of their two valence electrons, the level structure is much more complicated, making laser cooling harder, but possibly also opening up new possibilities. The element we wish to use for our new machine in Eindhoven is Sr. For a more extensive coverage of Sr, the reader is referred to [30]. Three of them are bosonic, with ^{88}Sr being the most abundant at $\sim$ 82.6%. There is one stable fermionic isotope: ^{87}Sr has a nuclear spin of $I = 9/2$ and an abundance of $\sim$ 7.0% [31]. This work is on ^{88}Sr. Because of the lack of hyperfine structure it simplifies a whole lot of things, but in principle one can work on all isotopes in the same machine as the energy splitting between the isotopes is in the MHz regime.

Strontium is also used in the best atomic clocks in the world [32], some for of the same reasons that it is a good candidate candidate for quantum computing, which we will discuss here.

2.2.1 Relevant Transitions

A simplified version of the level diagram of ^{88}Sr is shown in fig. 2.2. The notation is $(n_1 l_1 n_2 l_2)^{2S+1} L_J$ where $n_{1,2}$ is the principal and $l_{1,2} = s, p, d, \ldots$ the azimuthal quantum number. Furthermore S, L and J are the total spin, orbital angular momentum and total angular momentum respectively [33]. This level scheme shows 6 out of 7 lasers to be used in this experiment.

- 461 nm. Broad transition, meaning a strong scattering force (eq. (2.2) and short lifetime and quick cycling frequency. This is useful to slow down the hot atomic beam coming from the oven, as well as catching the atoms in a so called blue MOT with 'hot' temperatures of $\sim$ 1 mK.)
- 689 nm. Being much narrower than the blue transition, its Doppler temperature eq. (2.5) is much lower at 179 nK, although in practice cooling is limited by the recoil limit to some $\sim$ 1 μK [34, 30].
- 698 nm. The ultra-narrow clock transition (γ = 1 mK). Used in atomic clocks because of its spectroscopic accuracy [32]. It will turn out that this feature can be put to good use in quantum

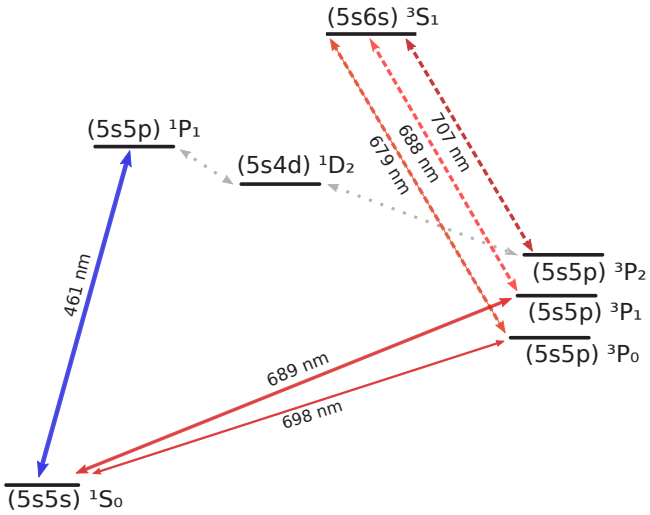

Fig. 2.2: Simplified level scheme for ^{88}Sr. Shown: blue transition for initial slowing and cooling. Narrower 689 nm transition of the red MOT, and the $^1S_0$ - $^3P_0$ clock transition, which we will be used to drive the qubits. To increase density and trap lifetime 3 repump lasers are used. Not shown: 813 nm dipole trapping laser because it is driven far off-resonant. Energies not to scale. Figure made by Ivo Knottnerus.

computers as well, and we will use it do coherently 'drive' the qubits between the qubit basis states. More about this in section 2.2.3

- 679, 688 and 707 nm. All repump lasers. 707 and 688 are used to cycle back atoms from ending up in $^3P_2$ from the decay channel showed by the grey dotted line in fig. 2.2. 679 is used to prevent repump leaks to $^3P_0$ [30, 35].

One wavelength is not shown, which is in fact the laser that will supply the most amount of power. This is the trapping laser, which determines the amount of single atoms and therefore qubits the machine can house. Using 813 nm, it is detuned so far from resonance that is not shown in fig. 2.2 This wavelength gives the same light shift for $^1S_0$ and $^3P_0$. This will be explained more thoroughly in section 2.3.

2.2.2 Laser Cooling and Trapping of Sr

Because of the melting temperature of Sr is 777 °C, to get any relevant vapor pressure, the Sr is heated in an oven after which it sublimates. To obtain a small atomic beam divergence, the atoms are directed along a bundle of capillary tubes with high aspect ratio [30].

Because of the oven, the atoms are moving way too fast to be efficiently captured by the MOT. Therefore, they are slowed by a Zeeman slower. This is a device similar to a MOT, but designed to cool only in one direction. A red-detuned laser is propagating in opposite direction of the atomic beam. A spatially varying magnetic field ensures a wide range of velocities is at some point resonant with the laser according to eq. (2.7).

Depending on the length of the Zeeman slower, only a fraction of the atoms will be slowed. To separate the hot from the cool atoms (the former are unwanted in a vacuum chamber) a deflection stage is used. The blue transition of Sr is used for this stage because of the strong scattering force. The Zeeman slowing and deflection stage is explained more elaborately in the thesis of Rik van Herk [36].

After the deflection stage, the atomic beam enters a glass cell. The advantage of using a glass cell is that is allows for the maximum amount of optical axis. To allow for longer trap survival times, the glass cell has ultra high vacuum (UHV) which is separated from the stages preceding it by a differential pumping stage.

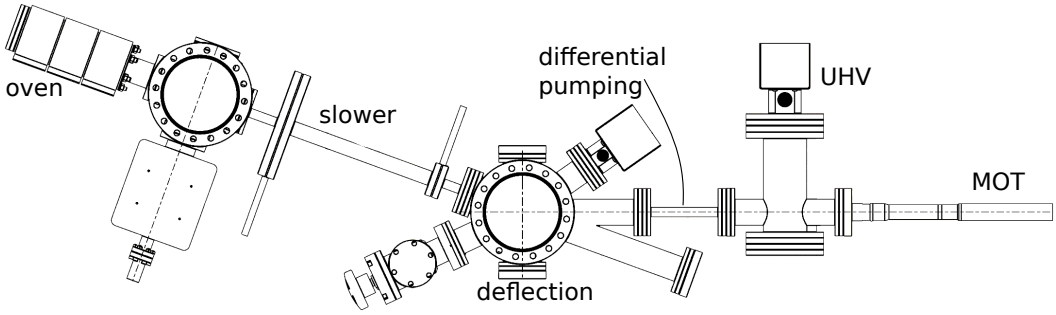

Fig. 2.3: Sketch of the vacuum atom source design and vacuum chambers. Starting from the oven, the atomic beam traverses a Zeeman slower, deflection stage and differential pumping stage before ending in the glass cell (MOT, right). Figure by Patrick de Laat.

2.2.3 Strontium as a Qubit

The main reason we want to use strontium atoms for the quantum processing unit is the $^3P_0$ state and its very long life time. The clock transition is forbidden according to selection rules, and only opens up after applying a magnetic field for the ^{88}Sr isotope, after which the lifetime is in the order of ~ 100 s. On the timescales of the operation of a quantum computer, we can therefore consider $^3P_0$ a 'second ground state'.

We aim to define the two clock states as our qubit manifold, such that we have:

$$\{|0\rangle, |1\rangle\} = \{|^1S_0\rangle, |^3P_0\rangle\} \tag{2.10}$$

Such that we have two long-lifetime states with a extremely narrow transition between them such that we can coherently drive between the qubit states. Because both states are 'ground' states, this type of scheme is called $|gg\rangle$ [27]. To entangle the qubits, Rydberg dressing can be used [27] where a small part of a Rydberg state $|r\rangle$ is admixed in one of the ground states.

$$|\psi\rangle \sim |g\rangle + \epsilon|r\rangle \tag{2.11}$$

The degree dressing is tuned by the (small) dressing parameter $\epsilon \propto \Omega/2\delta$ where Ω is the Rabi frequency of the laser and δ the usual detuning. A Rydberg state is an electronic state with very high principal quantum number n. Rydberg atoms are physically larger, as the electron orbit scales $\propto n^2$ [37]. As a result of these exaggerated electron orbit sizes, neighboring atoms can 'feel' each other. For example, the van der Waals interaction coefficient scales as $\propto n^{11}$ [37].

Other qubit implementations than the one above are possible as well. For example, [38] uses the fermionic ^{87}Sr and maps the qubit states onto the nuclear spin states $|^1S_0, F = 9/2, m_F = -9/2\rangle$ and $|^1S_0, F = 9/2, m_F = -7/2\rangle$ nuclear magnetic spin states.

2.3 Optical Dipole Traps

Now that the qubit manifold is known, we will talk about how to experimentally trap these qubits. While magneto optical traps are excellent for producing clouds of ultracold atoms, the constant photon scattering is unwanted during qubit operation. Therefore, after the atom cloud is cooled in the MOT, the MOT is typically overlapped with another type of trap: optical dipole trap (ODT). An ODT uses far off-resonant light and is therefore much weaker. However, because the light is off-resonant, such that scattering events are kept to a minimum and is thus non-destructive for coherence.

The light field $\mathbf{E}$ will induce a dipole moment $\mathbf{p}$ in the atom according to

$$\mathbf{p} = \alpha\mathbf{E} \tag{2.12}$$

in turn, the dipole potential will interact with the electric field leading to and an interaction dipole potential U_{dip}

$$U_{\text{dip}}(\mathbf{r}) = -\mathbf{pE} = -\frac{1}{2}\langle \mathbf{pE} \rangle = \frac{\text{Re}(\alpha)}{2\epsilon_0 c} I(\mathbf{r}) \tag{2.13}$$

where we have averaged the rapidly oscillating phase terms of the light, giving the factor $1/2$ and furthermore $I(\mathbf{r}) = |\mathbf{E}(\mathbf{r})|^2/(2\epsilon_0 c)$ where ϵ_0 is the electric constant. The dipole force thus scales with the in-phase part of the polarizability with the light field. An additional factor $1/2$ comes in because the dipole moment is induced and not permanent. The gradient of eq. (2.13) gives rise to the dipole force:

$$\mathbf{F}_{\text{dip}}(\mathbf{r}) = -\frac{\text{Re}(\alpha)}{2\epsilon_0 c} \nabla I(\mathbf{r}) \tag{2.14}$$

eq. (2.14) tells us that in order to maximize the dipole force, one has to maximize the gradient of the light intensity profile. This can be done by focussing the laser to the smallest possible spot, in order to achieve the highest possible dipole force. The scattering rate from the ODT can be found by averaging over the derivative of the dipole moment with the electric field

$$\Gamma_{\text{sc}}(\mathbf{r}) = \frac{\langle \mathbf{pE} \rangle}{\hbar\omega} = \frac{\text{Im}(\alpha)}{\hbar\epsilon_0 c} I(\mathbf{r}) \tag{2.15}$$

These expressions are true for any atom in a potential. The fact that α is complex means there is a phase delay between the electric field and the dipole response. The task that remains is finding the polarizability α. As a starting point, we will consider the electron as a harmonic oscillator with a damping coefficient. The dampening yields the polarizability, which for alkali atoms like Rb is accurate to within a few percent:

2.3.1 Classical

In the classical picture, we assume a classical light field, as well as a classical electron (harmonic oscillator). We can write down a general expression for the the light field propagating in the z-direction polarized in the $\hat{\epsilon}$ direction perpendicular to it:

$$\mathbf{E}(z,t) = \mathbf{E}_0 \cos(kz - \omega t)\hat{\epsilon} \tag{2.16}$$

The electron is modeled as a damped harmonic oscillator (Lorentz oscillator). Integrating the equation of motion for the electron, assuming a dipole moment $\mathbf{p} = e\mathbf{r}$ where r is the position yields after equating to eq. (2.12) for the polarizability [39]

$$\alpha = 6\pi\epsilon_0 c^3 \frac{\Gamma/\omega_0^2}{\omega_0^2 - \omega^2 - \text{i}\omega^3\Gamma/\omega_0^2} \tag{2.17}$$

,

Where Γ is the on-resonant damping rate in terms of the electron mass m_e.

$$\Gamma = \frac{e^2\omega_0^2}{6\pi\epsilon_0 m_e c^3} \tag{2.18}$$

Inserting eq. (2.17) in eqs. (2.13) and (2.15) yields, after assuming $\delta \ll \omega, \Gamma \ll \omega$

$$U_{\text{dip}}(\mathbf{r}) = \frac{3\pi c^2}{2\omega_0^3}\frac{\Gamma}{\delta} I(\mathbf{r}), \quad \Gamma_{\text{sc}}(\mathbf{r}) = \frac{3\pi c^2}{2\hbar\omega_0^3}\left(\frac{\Gamma}{\delta}\right)^2 I(\mathbf{r}) \tag{2.19}$$

The two parameters that we can control are the light intensity $I(\mathbf{r})$ and the detuning δ [39]. The relationship between them is $\hbar\Gamma_{sc} = \Gamma U_{\text{dip}}/\delta$. So in order to keep scattering events to a minimum and obtaining deep traps, we should use large detunings. To ensure the traps are deep, high light intensities are used.

2.3.2 Semi-Classical

In the semi-classical picture, we consider the same classical light field eq. (2.16), but consider an atom with quantized energy levels. We will consider a two level atom with eigenstates $|g\rangle$ (ground) with energy $\hbar\omega_g$ and $|e\rangle$ (excited) with $\hbar\omega_e$,see fig. 2.4a. Then the atomic Hamiltonian in this basis reduces to [40]

$$\mathcal{H}_A = \hbar\omega_g|g\rangle\langle g| + \hbar\omega_e|e\rangle\langle e| \tag{2.20}$$

The radiation field is modeled as a time-dependent perturbation such that the total Hamiltonian is [41]

$$\mathcal{H} = \mathcal{H}_A + \mathcal{H}_I(t), \tag{2.21}$$

We can write down the wave function in the basis of the atomic eigenstates, and their time-evolution is now given by

$$|\psi\rangle = c_g(t)e^{-i\omega_g t}|g\rangle + c_e(t)e^{-i\omega_e t}|e\rangle. \tag{2.22}$$

In appendix B the Schrodinger equation is solved for the 2-level atom using the dipole approximation as well as the rotating wave approximation (RWA). The following matrix equation is derived for the 2 level atom (fig. 2.4a) [42]

$$i\hbar\begin{pmatrix}\dot{c}_g\\ \dot{c}e\end{pmatrix} = \frac{\hbar}{2}\begin{pmatrix}\delta & \Omega\\ \Omega^* & -\delta\end{pmatrix}\begin{pmatrix}c_g\\ c_e\end{pmatrix} \tag{2.23}$$

.

where the coupling between the atomic eigenstates and the radiation field is described by the Rabi frequency:

$$\Omega \equiv \frac{eE_0}{\hbar}\langle g|\mathbf{r}|e\rangle \tag{2.24}$$

The Hamiltonian of eq. (2.23) has eigenvalues

$$E_\pm = \frac{1}{2}\sqrt{\Omega^2 + \delta^2} \tag{2.25}$$

. Assuming $|\delta| \gg \Omega$, the eigenenergies are thus

$$E_g = \frac{\hbar\delta}{2} + \frac{\hbar\Omega^2}{4\delta}, \quad E_e = \frac{\hbar\delta}{2} - \frac{\hbar\Omega^2}{4\delta} \tag{2.26}$$

When turning on the laser, the energies are thus shifted by an amount $\Delta E = E(\Omega) - E(\Omega = 0)$ And it turns out the eigenenergies are shifted by an amount known as the light shift or AC stark shift [43]

$$\Delta E_{e,g} = \pm\frac{\hbar\Omega^2}{4\delta}. \tag{2.27}$$

The light shift is proportional to the light intensity over the detuning: $\Omega^2/\delta \propto I/\delta$, which we already found for the classical treatment in eq. (2.19). This behavior is shown in fig. 2.4b. Because the field is off-resonant, atoms only occupy the ground state. For $\delta < 0$ ('red-detuned'), the ground state light state is negative. To calculate the new eigenstates, we repeat the treatment for a quantized light field, known as the dressed state picture.

2.3.3 Dressed Atom Approach

To calculate the new shifted eigenstates, the full Hamiltonian has to be considered, included a quantized light field with Hamiltonian $\mathcal{H}_L$ [44]

$$\mathcal{H} = \mathcal{H}_A + \mathcal{H}_L + \mathcal{H}_I(t) \tag{2.28}$$

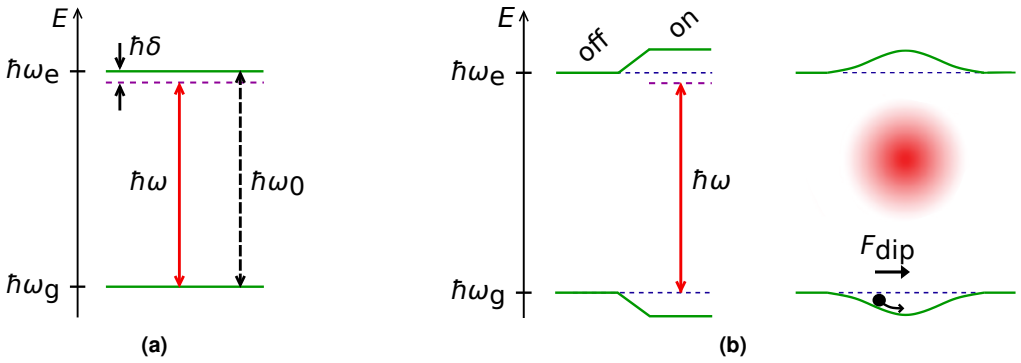

Fig. 2.4: a) Energy level scheme for the 2-level case. The two energies are split by $\omega_e - \omega_g = \omega_0$. The detuning is $\delta = \omega - \omega_0$. b) Light shift when the off-resonant laser is turned on, as well as the spatially varying light shift for a laser beam profile. Figure adapted from [39]

where the light field has eigenenergies separated by the photon energy and eigenstates of n photons: $|n\rangle$ [43]

$$\mathcal{H}_L = \sum_n \hbar\omega \left(n + \frac{1}{2}\right) |n\rangle\langle n| \tag{2.29}$$

The new eigenstates are

$$\begin{aligned} |1\rangle &= \cos\theta|g,n\rangle - \sin\theta|e,n-1\rangle, \\ |2\rangle &= \sin\theta|g,n\rangle + \cos\theta|e,n-1\rangle \end{aligned} \tag{2.30}$$

where the mixing angle θ is $\cos(2\theta) = -\delta/\sqrt{\delta^2 + \Omega^2}$

Chapter 3

Making Optical Tweezers

Chapter 4

Generating Tweezer Arrays

Chapter 5

Implementation in the Machine

Chapter 6

Conclusions and Outlook

Bibliography

[1] G. E. Moore. “Cramming more components onto integrated circuits”. Tech. rep. Electronics Magazine. 1965.

[2] R. P. Feynman. “Simulating physics with computers”. In: *Int. J. Theor. Phys.* 21.6 (1982), pp. 467–488–467–488. DOI: 10.1007/BF02650179.

[3] A. Robert et al. “Resource-efficient quantum algorithm for protein folding”. In: *npj Quantum Inf.* 7.1 (2021), p. 38. DOI: 10.1038/s41534-021-00368-4.

[4] H. Ma, M. Govoni, and G. Galli. “Quantum simulations of materials on near-term quantum computers”. In: *npj Computational Materials* 6.1 (2020), p. 85. DOI: 10.1038/s41524-020-00353-z.

[5] D. J. Griffiths. *Introduction to Quantum Mechanics (2nd Edition)*. Pearson Prentice Hall, Apr. 2004.

[6] M. A. Nielsen and I. L. Chuang. *Quantum Computation and Quantum Information: 10th Anniversary Edition*. Cambridge University Press, 2011.

[7] J. A. Jones and D. Jaksch. *Quantum Information, Computation and Communication*. English. Cambridge, UK: Cambridge University Press, 2012.

[8] L. Henriet et al. “Quantum computing with neutral atoms”. In: *Quantum* 4 (Sept. 2020), p. 327. DOI: 10.22331/q-2020-09-21-327.

[9] D. P. DiVincenzo. “The Physical Implementation of Quantum Computation”. In: *Fortschr. Phys.* 48.9-11 (Sept. 2000), pp. 771–783.

[10] A. Peres. “Reversible logic and quantum computers”. In: *PRA* 32.6 (Dec. 1985), pp. 3266–3276. DOI: 10.1103/PhysRevA.32.3266.

[11] T. D. Ladd et al. “Quantum computers”. In: *Nature* 464.7285 (2010), pp. 45–53. DOI: 10.1038/nature08812.

[12] J. Preskill. “Quantum Computing in the NISQ era and beyond”. In: *Quantum* 2 (Aug. 2018), p. 79. DOI: 10.22331/q-2018-08-06-79.

[13] A. Peruzzo et al. “A variational eigenvalue solver on a photonic quantum processor”. In: *Nat Commun* 5.1 (2014), pp. 4213–4213. DOI: 10.1038/ncomms5213.

[14] J. R. McClean et al. “The theory of variational hybrid quantum-classical algorithms”. In: *New J. Phys.* 18.2 (Feb. 2016), p. 023023. DOI: 10.1088/1367-2630/18/2/023023.

[15] N. Moll et al. “Quantum optimization using variational algorithms on near-term quantum devices”. In: *Quantum Science and Technology* 3.3 (2018), p. 030503. DOI: 10.1088/2058-9565/aab822.

[16] J. C. F. Matthews et al. “Manipulation of multiphoton entanglement in waveguide quantum circuits”. In: *Nat. Photonics* 3.6 (2009), pp. 346–350–346–350. DOI: 10.1038/nphoton.2009.93.

[17] J. Benhelm et al. “Towards fault-tolerant quantum computing with trapped ions”. In: *Nat. Phys.* 4.6 (Apr. 2008), pp. 463–466–463–466. DOI: 10.1038/nphys961.

[18] P. Schindler et al. “A quantum information processor with trapped ions”. In: *New Journal of Physics* 15.12 (2013), p. 123012. DOI: 10.1088/1367-2630/15/12/123012.

[19] D. Press et al. “Complete quantum control of a single quantum dot spin using ultrafast optical pulses.” In: *Nature* 456 (Nov. 2008), pp. 218–21.

[20] L. DiCarlo et al. “Demonstration of two-qubit algorithms with a superconducting quantum processor”. In: *Nature* 460.7252 (2009), pp. 240–244–240–244. DOI: 10.1038/nature08121.
[21] F. Arute et al. “Quantum supremacy using a programmable superconducting processor”. In: *Nature* 574.7779 (2019), pp. 505–510–505–510. DOI: 10.1038/s41586-019-1666-5.
[22] S. Chu et al. “Experimental Observation of Optically Trapped Atoms”. In: *PRL* 57.3 (1986), pp. 314–317–314–317. DOI: 10.1103/PhysRevLett.57.314.
[23] N. Schlosser et al. “Sub-poissonian loading of single atoms in a microscopic dipole trap”. In: *Nature* 411.6841 (2001), pp. 1024–1027. DOI: 10.1038/35082512.
[24] S. Bergamini et al. “Holographic generation of microtrap arrays for single atoms by use of a programmable phase modulator”. In: *J. Opt. Soc. Am. B* 21.11 (2004), pp. 1889–1894–1889–1894. DOI: 10.1364/JOSAB.21.001889.
[25] H. Levine et al. “High-Fidelity Control and Entanglement of Rydberg-Atom Qubits”. In: *PRL* 121.12 (Sept. 2018), p. 123603. DOI: 10.1103/PhysRevLett.121.123603.
[26] I. S. Madjarov et al. “High-fidelity entanglement and detection of alkaline-earth Rydberg atoms”. In: *Nat. Phys.* 16.8 (2020), pp. 857–861. DOI: 10.1038/s41567-020-0903-z.
[27] X. Wu et al. “A concise review of Rydberg atom based quantum computation and quantum simulation*”. In: *Chinese Physics B* 30.2 (2021), p. 020305. DOI: 10.1088/1674-1056/abd76f.
[28] H. J. Metcalf and P. van der Straten. *Laser Cooling and Trapping*. New York: Springer-Verlag, 1999.
[29] K. Kowalski et al. “Magneto-optical Trap: Fundamentals and Realization”. In: *Computational Methods in Science and Technology* Vol. spec. iss. (2) (2010), pp. 115–129.
[30] S. Stellmer. “Degenerate quantum gases of strontium”. PhD thesis. University of Innsbruck, 2013.
[31] J. S. Coursey, D. J. Schwab, and R. A. Dragoset. *Atomic Weights and Isotopic Compositions*. NIST. 1999. URL: https://www.nist.gov/pml/atomic-and-molecular-data.
[32] B. J. Bloom et al. “An optical lattice clock with accuracy and stability at the 10e-18 level”. In: *Nature* 506.7486 (2014), pp. 71–75. DOI: 10.1038/nature12941.
[33] R. Cowan. *The Theory of Atomic Structure and Spectra*. Berkele: University of California Press, 1981.
[34] M. M. Boyd. “High Precision Spectroscopy of Strontium in an Optical Lattice: Towards a New Standard for Frequency and Time”. PhD thesis. University of Colorado, 2007.
[35] X. Xu et al. “Cooling and trapping of atomic strontium”. In: *J. Opt. Soc. Am. B* 20.5 (2003), pp. 968–976. DOI: 10.1364/JOSAB.20.000968.
[36] R. van Herk. “Simulating trajectories of 88Sr atoms in a laser cooling machine”. MA thesis. Eindhoven University of Technology, 2022.
[37] T. F. Gallagher. *Rydberg Atoms*. Cambridge: Cambridge University Press, 1994. DOI: 10.1017/CBO9780511524530.
[38] K. Barnes et al. “Assembly and coherent control of a register of nuclear spin qubits”. Aug. 2021. DOI: https://arxiv.org/abs/2108.04790.
[39] R. Grimm et al. “Optical Dipole Traps for Neutral Atoms”. In: *Advances In Atomic, Molecular, and Optical Physics*. Vol. 42. Academic Press, 2000, pp. 95–170. DOI: 10.1016/S1049-250X(08)60186-X.
[40] R. Loudon. *The quantum theory of light, 3rd ed*. Oxford University Press, 2000.
[41] T. van Leeuwen. *Lecture notes Advanced Optics Part I: Theory*. 2017.
[42] C. Foot. *Atomic Physics*. Oxford University Press, 2005.
[43] E. J. D. Vredenbregt. *Lectures on Ultracold Quantum Physics*. June 2020.
[44] J. Dalibard and C. Cohen-Tannoudji. “Dressed-atom approach to atomic motion in laser light: the dipole force revisited”. In: *J. Opt. Soc. Am. B* 2.11 (1985), pp. 1707–1720. DOI: 10.1364/JOSAB.2.001707.
[45] R. LaRose. *Expectation Values, Quantum Information and Computing Seminar*. Jan. 2021.

Appendices

Appendix A

Pauli Strings

In VQE, the Hamiltonian is decomposed in Pauli strings P_α.

$$\mathcal{H} = \sum_\alpha h_\alpha P_\alpha \tag{A.1}$$

A Pauli string is a tensor product of Pauli matrices $\sigma_j^\alpha \in \{\mathcal{I}, \sigma_j^x, \sigma_j^y, \sigma_j^z\}$ where $\mathcal{I}$ is the identity matrix and σ_j^α are the standard Pauli spin matrices [5]

$$\mathcal{I} = \begin{pmatrix} 1 & 0 \\ 0 & 1 \end{pmatrix}, \quad \sigma_j^x = \begin{pmatrix} 0 & 1 \\ 1 & 0 \end{pmatrix}, \quad \sigma_j^y = \begin{pmatrix} 0 & -i \\ i & 0 \end{pmatrix} \quad \text{and} \quad \sigma_j^z = \begin{pmatrix} 1 & 0 \\ 0 & -1 \end{pmatrix} \tag{A.2}$$

Such that the Pauli string is [15]:

$$P_\alpha = \sigma_1^{\alpha_1} \otimes \sigma_2^{\alpha_2} \otimes \ldots \otimes \sigma_N^{\alpha_N} = \bigotimes_{j=1}^{N} \sigma_j^{\alpha_j} \tag{A.3}$$

This has the nice property that estimating the Hamiltonian is equivalent to measuring populations of individual qubits. This has to be done repeatedly, in order to get an estimate. Using the definition for the expectation value for σ_j^z for example yields

$$\langle\psi|\sigma_j^z|\psi\rangle = \begin{pmatrix} a & b \end{pmatrix}^\dagger \begin{pmatrix} 1 & 0 \\ 0 & -1 \end{pmatrix} \begin{pmatrix} a \\ b \end{pmatrix} = |a|^2 - |b|^2 \tag{A.4}$$

Expectation values of tensor products of Pauli strings can be found in a similar fashion [45]. For a string of 2 Pauli matrices, for example σ_j^x and σ_j^y, use need the two qubit definition eq. (1.3) to find

$$\langle\psi_{2q}|(\sigma_j^x \otimes \sigma_j^y)|\psi_{2q}\rangle = |\alpha_{00}|^2 - |\alpha_{01}|^2 - |\alpha_{10}|^2 + |\alpha_{11}|^2. \tag{A.5}$$

Appendix B

Light Matter Interaction

We follow [41]. For a 2-level atom (see fig. 2.4a), the atomic Hamiltonian is best written down in its eigenstates, such that we have

$$\mathcal{H}_A = \hbar\omega_g|g\rangle\langle g| + \hbar\omega_e|e\rangle\langle e| \tag{B.1}$$

Where the eigenvalues are $\hbar\omega_g$ and $\hbar\omega_e$, and they satisfy the Schrodinger equation

$$i\hbar|\dot{g}\rangle = \hbar\omega_g|g\rangle, \tag{B.2a}$$
$$i\hbar|\dot{e}\rangle = \hbar\omega_e|e\rangle \tag{B.2b}$$

Where the dote denotes the temporal derivative. We treat the light field as a time dependent perturbation $H_I(t)$ such that the total Hamiltonian is

$$\mathcal{H} = \mathcal{H}_A + \mathcal{H}_I(t), \tag{B.3}$$

The time evolution of eq. (B.3) can be written down in the unperturbed states as

$$|\psi\rangle = c_g(t)e^{-i\omega_g t}|g\rangle + c_e(t)e^{-i\omega_e t}|e\rangle. \tag{B.4}$$

Substituting eqs. (B.3) and (B.4) in the Schrodinger equation yields, after canceling the terms that involve eq. (B.2)

$$i\hbar\left(\dot{c}_g(t)e^{-i\omega_e t} + \dot{c}_e(t)e^{-i\omega_e t}\right) = c_g(t)\mathcal{H}_I(t)|g\rangle e^{-i\omega_g t} + c_e(t)\mathcal{H}_I(t)|e\rangle e^{-i\omega_e t}, \tag{B.5}$$

Because $\{|g\rangle, |e\rangle\}$ constitute an orthogonal set, we can exploit a trick where we multiply eq. (B.5) from the left by $\{\langle g|, \langle e|\}$, yielding a set of two coupled equations:

$$i\hbar\dot{c}_g = e^{-i\omega_0 t}\left[c_g\langle g|\mathcal{H}_I|g\rangle + c_e\langle g|\mathcal{H}_I|e\rangle\right] \tag{B.6a}$$
$$i\hbar\dot{c}_e = e^{i\omega_0 t}\left[c_g\langle e|\mathcal{H}_I|g\rangle + c_e\langle e|\mathcal{H}_I|e\rangle\right]. \tag{B.6b}$$

Where the explicit time dependence of c_g and c_e will be omitted from now on. In order to calculate the matrix elements in eq. (B.6), the Wigner-Eckart theorem can be used. If $|g\rangle$ and $|e\rangle$ are described by the quantum numbers J, M and α (total and magnetic quantum number, and α keeps track of the other quantum numbers), the matrix element can be evaluated as

$$\langle J_g M_g \alpha_g|\hat{T}^n_q|J_e M_e \alpha_e\rangle = (-1)^{J_e - M_e}\begin{pmatrix} J_e & n & J_g \\ -M_e & q & M_1\end{pmatrix}\langle J_g\alpha_e||\hat{T}^n||J_g\alpha_g\rangle \tag{B.7}$$

Where $q \in \{-1, 0, 1\}$ is the spherical component index, the 2 x 3 matrix is the $3j$-symbol, which is

in principle known and can be formulated in terms of Glebsch-Gordan coefficients. $\hat{T}^n_q$ is the a spherical tensor operator. The term $\langle||\hat{T}^n||\rangle$ is the reduced matrix element [41]. Calculating the matrix elements will not be done here, but many $3j$-symbols will turn out to be zero. For example, the diagonal matrix elements will turn out to be zero, such that eq. (B.6) reduces to

$$i\hbar\dot{c}_g = e^{-i\omega_0 t} c_e \langle g|\mathcal{H}_I|e\rangle \tag{B.8a}$$
$$i\hbar\dot{c}_e = e^{i\omega_0 t} c_g \langle e|\mathcal{H}_I|g\rangle. \tag{B.8b}$$

We will now calculated the matrix elements for the classical light field. Up until this point, the derivation was exact for the 2-level atom. Now we will make a series of approximations to get to a solvable set of equations [41]

$$\mathbf{E}(z,t) = \mathbf{E}_0 \cos(kz - \omega t) \tag{B.9}$$

Under the dipole approximation, the interaction Hamiltonian is [42]

$$\mathcal{H}_I = -e\mathbf{r}\cdot\mathbf{E} \tag{B.10}$$

Because an atom is orders of magnitude smaller than the wavelength of the radiation field, we can safely set $z = 0$. The Hamiltonian simplifies to

$$\mathcal{H}_I = \frac{-eE_0 z}{2}\left(e^{i\omega t} + e^{-i\omega t}\right) \tag{B.11}$$

Substitution of eq. (B.11) in eq. (B.8) yields

$$i\hbar\dot{c}_g = \frac{eE_0}{2} c_e [e^{i(\omega-\omega_0)t} + e^{-i(\omega+\omega_0)t}]\langle g|z|e\rangle \tag{B.12a}$$
$$i\hbar\dot{c}_e = \frac{eE_0}{2} c_g [e^{+i(\omega+\omega_0)t} + e^{-i(\omega-\omega_0)t}]\langle e|z|g\rangle. \tag{B.12b}$$

We assume $\omega \gg \delta$, such that $\omega + \omega_0 \approx 2\omega_0$ which oscillates much faster than the $\omega - \omega_0 = \delta$ term. Over time scales of absorption and emission processes, this much faster contribution averages out. This is known as the rotating wave approximation (RWA) [43, 40] Thus we are left with

$$i\hbar\dot{c}_g = c_e \frac{\hbar\Omega}{2} e^{i\delta t}, \tag{B.13a}$$
$$i\hbar\dot{c}_e = c_g \frac{\hbar\Omega^*}{2} e^{-i\delta t}. \tag{B.13b}$$

Where the so-called Rabi frequency

$$\Omega \equiv \frac{eE_0}{\hbar}\langle g|\mathbf{r}|e\rangle \tag{B.14}$$

and its complex conjugate is introduced. In order to remove the time-dependence of eq. (B.13), we can turn 'look' at them from a 'rotating frame'. More formally, it is a basis transformation described by the unitary matrix $\mathcal{U}$ [42]

$$\begin{pmatrix}\tilde{c}_g\\ \tilde{c}_e\end{pmatrix} = \mathcal{U}\begin{pmatrix}c_g\\ c_e\end{pmatrix} = \begin{pmatrix}e^{i\delta t/2} & 0\\ 0 & e^{-i\delta t/2}\end{pmatrix}\begin{pmatrix}c_g\\ c_e\end{pmatrix} = \begin{pmatrix}c_g e^{-i\delta t/2}\\ c_e e^{i\delta t/2}\end{pmatrix} \tag{B.15}$$

.

Substituting eq. (B.15) in eq. (B.13) yields, after omitting the tiles, the matrix equation eq. (2.23)

$$i\hbar\begin{pmatrix}\dot{c}_g\\ \dot{c}e\end{pmatrix} = \frac{\hbar}{2}\begin{pmatrix}\delta & \Omega\\ \Omega^* & -\delta\end{pmatrix}\begin{pmatrix}c_g\\ c_e\end{pmatrix}. \tag{B.16}$$